ARTICLES

Site-Dependent Spectral Shifts in Core-to-π^* Excitations of Pyridine Clusters†

I. L. Bradeanu‡ and N. Kosugi

Institute for Molecular Science, Okazaki 444-8585, Japan

R. Flesch and E. Rühl*

Physikalische und Theoretische Chemie, Institut für Chemie und Biochemie, Fachbereich Biologie, Chemie, Pharmazie, Freie Universität Berlin, Takustr. 3, 14195 Berlin, Germany

Received: March 9, 2008; Revised Manuscript Received: May 20, 2008

Site- and element-selective core-to-π^* excitation in free pyridine clusters is investigated. The experimental results indicate the occurrence of site- and size-dependent spectral shifts in the C 1s and N 1s $\rightarrow \pi^*$ excitation regime. Specifically, we observe in the C 1s regime a substantial and site-dependent redshift of the low energy slopes of the C 1s $\rightarrow \pi^*$ band by 90 meV in clusters relative to the bare molecule, whereas the high energy slopes of this band remain almost unchanged. In contrast, a size-dependent blueshift of the same order of magnitude is found for the entire N 1s $\rightarrow \pi^*$ band. This is distinctly different from previous results on van der Waals clusters, where exclusively redshifts in 1s $\rightarrow \pi^*$ transitions are observed. The experimental results are compared to ab initio calculations, which serve to simulate the 1s $\rightarrow \pi^*(\upsilon = 0)$ transitions. These results clearly indicate that the spectral shifts are primarily a result of electrostatic interactions between the molecular moieties and that an antiparallel orientation of molecular units preferably dominates in variable-size pyridine clusters.

Introduction

Intermolecular interactions between aromatic molecules have been investigated in the past, because they are of fundamental interest and they are of importance to biomolecular assemblies and materials research via molecular self-assemblies.[1–5] Electronic properties of free van der Waals clusters containing $\pi-\pi$ interactions have received specific interest, because these permit to investigate fundamental aspects on size-dependent properties of aromatic molecules. This includes ionization energies and ionization mechanisms,[6,7] microsolvation,[8] multiphoton ionization and Coulomb explosion by short pulse lasers,[9] and photoionization of size-selected anions.[10]

Core-level excitation of free clusters has contributed element-selective excitation, which is also size- and site-selective.[11] This allows one to study changes in the local electronic of free atomic and molecular clusters. It has been observed that the lowest core Rydberg states undergo upon conversion into the corresponding surface- and bulk-excitons substantial spectral shifts to higher energy, corresponding to a blueshift.[12–14] More recent work on Rydberg states of core-excited molecular clusters indicates that the experimentally observed spectral blueshifts are tightly related to the molecular orientation within a cluster.[15] These findings are unlike core-to-valence transitions in molecular clusters occurring below the core ionization energies, where specifically 1s$\rightarrow\pi^*$ transitions of unsaturated molecules and molecular clusters were investigated.[16,17] These show a slight redshift of $\leq$5 meV, which is a result of stabilization of the π^*-state in clusters. Similar findings have been reported more recently for low-lying continuum resonances, as observed in SF_6 clusters.[18] In contrast, substantial blueshift is observed for 1s$\rightarrow\sigma^*$ transitions, which is rationalized in terms of dynamic localization.[19]

Recently, we have investigated the C 1s$\rightarrow\pi^*$ excitation in variable-size benzene clusters.[20] These core-excited states undergo substantial redshifts up to 60 meV relative to the isolated molecule, which is larger by an order of magnitude than those observed in clusters of diatomic molecules.[16,17] This redshift occurring in benzene clusters is due to the core-excited benzene polarized by a localized core hole, as is supported by ab initio calculations on the C 1s$\rightarrow\pi^*(\upsilon = 0)$ excited clusters. Our previous work[20] also attempted to derive the gas-to-solid shift of core-excited benzene, which is not accurately known (cf. ref 21).

The present work on the near-edge structure of core-excited pyridine and its clusters is motivated by the fact that the carbon and nitrogen sites permit element-selective excitations of the aromatic ring system, which is a result of the different absorption energies between the C 1s- and the N 1s-absorption edges. It is anticipated that this element-selective excitation can be exploited to probe the molecular orientation in pyridine clusters in a selective way. We combine in this study experimental and theoretical work on the C and N 1s$\rightarrow\pi^*$ excitations of variable-size pyridine clusters. It is also of interest to show whether different stabilization shifts occur in clusters upon element-

† Part of the "Stephen R. Leone Festschrift".

* Corresponding author. Tel: ++49-30-8385 2396. Fax: ++49-30-8385 2717. E-mail: ruehl@chemie.fu-berlin.de.

‡ Present address: Department of Physics, Uppsala University, Box 530, S-751 21 Uppsala, Sweden.

10.1021/jp802068h CCC: $40.75
Published on Web 07/19/2008

selective excitation, that is, in the C 1s→π^* and N 1s→π^* excitation regimes.

Experimental Section

The experimental setup consists of a supersonic jet expansion that is used for cluster production and a time-of-flight mass spectrometer for cation separation and detection. Details of this setup have been published elsewhere.[20,22] This setup is mounted at the UE52-SGM beam line of the storage ring BESSY (Berlin, Germany), where monochromatic synchrotron radiation in the soft X-ray regime is delivered for photoexcitation and photoionization of neutral, variable-size pyridine clusters. The energy resolving power $E/\Delta E$ is set to ≥6 000. The photon energy scale is calibrated according to previous results on molecular pyridine.[23] Clusters are formed in a coexpansion of argon and pyridine, where the seeded beam technique is used.[24] The gas mixture is expanded at room temperature with moderate stagnation pressures ranging between 1 and 2 bar. Such mild expansions lead preferentially to homogeneous cluster formation. The size regime explored in this work focuses on small clusters, containing ≤20 molecules per cluster. There is no evidence for the occurrence of heteroclusters, as evidenced by photoionization mass spectra, where no mass lines from heterogeneous clusters are observed. This result is also consistent with recent work on benzene clusters, where photoion yields in the Ar 2p regime indicated via element-selective detection that there is no argon bound in clusters containing aromatics.[20] The pyridine and argon samples are of commercial quality. They are used without purification. Cations are formed by photoionization in the soft X-ray regime. They are separated in a time-of-flight mass spectrometer.[22] Photoion yields of the molecular fragments that are centered in the mass range near $m/z \approx 50$, corresponding to $C_3H_xN^+/C_4H_x^+$, are not affected by fragmentation of clusters. This is similar to previous work on benzene clusters.[20] Therefore, we use this range of mass channels for probing molecular properties. We have measured simultaneously the pyridine dimer cation yield, which is indicative for the electronic structure of clusters. Note that different mass channels that are populated by cluster fragmentation show similar results in near-edge spectra, implying that the final ionic fragmentation channels do not yield size-dependent electronic properties at constant expansion conditions. An efficient way to probe size effects in electronic structure is to change the expansion conditions, as done in the present and previous work.[20] The experiments cover the regimes of the C 1s and N 1s absorption edges, similarly to previous work.[15–18,20,22] This provides photoion yields, which reflect changes in electronic properties upon cluster formation, as outlined in our previous work on benzene clusters.[20]

Theoretical Model

Full geometry optimization for the pyridine dimers, trimers, and tetramers at the MP2 6-311G** levels are performed with the Gaussian program package.[25] The core-to-π^* excited states of those optimized geometries are solved within the Hartree−Fock approximation by explicitly taking the core hole into account. This is accomplished by using the GSCF3 program package, which makes it possible to keep from variational collapse to lower states within one-Hamiltonian and partial self-consistent field (SCF) schemes.[26–28] Primitive basis functions are taken from the (73/7) and (63/5) contracted Gaussian-type functions of Huzinaga et al.[29] They are augmented with d-type polarization functions $\zeta_d = 0.617$ for C and N atoms. The contraction scheme is an extended basis set (3111121/31111/1) for the ionized C and N atoms and a split-valence basis set of double ζ quality (621/41/1) for the neutral C atoms and (32) for H atoms. Diffuse functions are not included, because Rydberg states are not considered in the present work. The core-to-π^* calculations ignore the zero-point vibrational energy and the electron correlation energy involving the intermolecular van der Waals or dispersion interactions. It is expected that these are canceled between the electronic ground state and the core excited state. A separate calculation is performed for each distinct atomic site for all stable isomers by using GSCF3.

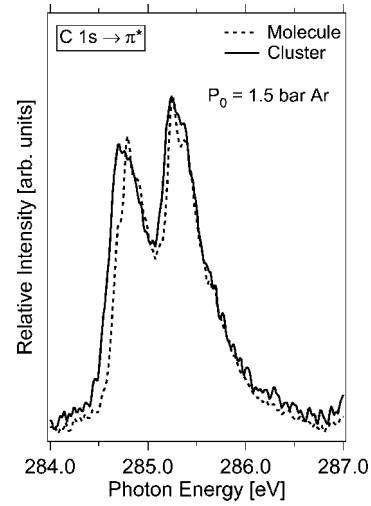

Figure 1. C 1s excitation regime of molecular (dashed curve) and clustered pyridine (solid curve). Experimental conditions: $p_0 = 1.5$ bar; $T_0 = 300$ K; seed gas, Ar.

Experimental Results and Discussion

Photoionization mass spectra of pyridine clusters have been measured in the C 1s and N 1s excitation regimes. The mass spectra show, similarly to previous work on valence shell excitation,[6,30] singly charged cluster mass lines. We have used the dimer cation mass signal in order to detect electronic properties of clusters as a function of cluster size. Molecular properties are measured simultaneously by using the $m/z \approx 50$ mass signal. This approach is known to yield reliably spectral shifts in the core level excitation regime.[17,18,20,22] The results are shown in Figures 1–3.

C 1s→π^* Regime. Figure 1 shows the C 1s→π^* (b_1) regime between 284 and 287 eV, which is split as a result of the considerable difference in excitation energies between the carbon sites that are located in different positions relative to the nitrogen site. The para and meta sites contribute mostly to the low-energy feature of this C 1s→π^* band, whereas the high-energy portion of the band is known to be due to the ortho-carbon sites.[23] Similar results have been derived from earlier high-resolution electron energy loss spectra and model calculations.[31] Figure 1 also indicates that the C 1s→π^* transition of both the molecule and clusters is similar in shape compared to that obtained in earlier work.[23,31] However, if one carefully looks at the separation of both C 1s→π^* features, it becomes evident that they are more resolved in the present work. This is ascribed to the improved energy resolution of the present experiments. Furthermore, the separation of both bands remains almost unchanged in molecules and clusters. The high-energy slopes of the split band is almost identical in the molecules and in clusters, whereas the lowest energy slope near 284.5 eV is clearly red shifted in clusters relative to the isolated molecule by 90 meV. A smaller shift is observed for the low-energy slope of the C 1s(ortho)→π^* feature. This leads as a net result to an

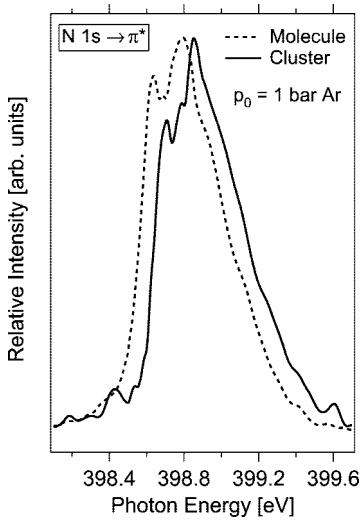

Figure 2. N 1s excitation regime of molecular (dashed curve) and clustered pyridine (solide curve). Experimental conditions: $p_0 = 1$ bar; $T_0 = 300$ K; seed gas, Ar.

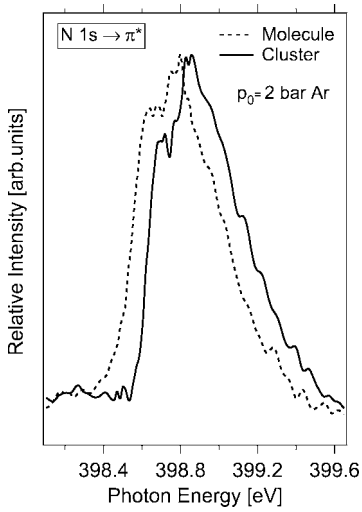

Figure 3. N 1s excitation regime of molecular (dashed curve) and clustered pyridine (solid curve). Experimental conditions: $p_0 = 2$ bar; $T_0 = 300$ K; seed gas, Ar.

asymmetric broadening of the features in clusters. These findings are discussed below in comparison with ab initio calculations.

N 1s→π* Regime. The regime of the N 1s→π* (b_1) transition is shown in Figures 2 and 3, where different expansion conditions are chosen for cluster production. The molecular spectrum is included for a comparison. It shows weak features near the maximum of the band. These have not been observed in previous high-resolution work.[23,31] This is a result of the improved energy resolution. The features are likely due to vibronic fine structure near the Franck−Condon maximum of the band. The cluster spectrum displayed in Figure 2 is recorded at a stagnation pressure p_0 of 1 bar, whereas the spectrum shown in Figure 3 is recorded at $p_0 = 2$ bar. Argon is used in both experiments as a seed gas, where the stagnation pressure is known to increase the average cluster size that is formed in the expansion (cf. ref 20). A comparison of Figures 2 and 3 allows one to estimate the cluster-size dependence of the spectra features, similarly to recent work on C 1s excited benzene clusters.[20] This assumption appears to be plausible, because model calculations on benzene and pyridine dimers reveal similarly stacked structures.[32] This is due to the fact that in pyridine dimers, the electrostatic contribution accounts only for 1 kcal mol^{-1}.[32] The structures of pyridine dimers and clusters will be shown further below. Furthermore, it is well-known that it is difficult to estimate the average cluster size of molecular clusters from the expansion conditions.[33,34] The cluster size contributing to the experimental spectra shown in Figures 2 and 3 is estimated similarly to previous work on benzene clusters.[20] Core-level excitation produces efficiently doubly charged clusters via Auger decay processes. These are known to be stable for $\geq$23 molecular moieties per cluster.[35] We assume that the critical size for doubly charged pyridine clusters is of the same order of magnitude. Then, the dimer cation signal, that has massive contributions from larger clusters via ionic fragmentation, corresponds to clusters containing less than about 20 molecules. Larger clusters are not observed in photoionization mass spectra. Evidently, they are not probed by the approach of photoion yields, even though they may be formed in the jet. Therefore, it appears to be straightforward to focus in the following on model structures of small clusters in order to simulate the experimental results. These are discussed in the following section.

A comparison of the experimental spectra corresponding to molecules and clusters in the N 1s regime indicates a different behavior from that in the C 1s regime. It is evident that in the N 1s regime, the entire N 1s→π* (b_1) band is blueshifted in clusters. The fine structure near the maximum of the band remains unchanged, if one considers the limited signal-to-noise ratio in the results from clusters. The blueshift indicates that there is a slight size dependence. We observe at $p_0 = 1$ bar a blueshift of 85 $\pm$ 15 meV (see Figure 2), which increases to 95 $\pm$ 15 meV at $p_0 = 2$ bar (see Figure 3). The magnitude of spectral shift is similar to that of the C 1s regime (see above), and it is substantially larger than in C 1s excited benzene clusters.[20] Note that these spectral shifts of the core-to-valence transitions are substantially larger than those observed in previous work on clusters of diatomic molecules, where spectral shifts $\leq$5 meV were observed.[16,17] Furthermore, the N 1s→ π* (b_1) transition is the first example of a core-to-valence transition below a core ionization energy that undergoes a destabilization in clusters relative to the bare molecule. The origin of these differences is also discussed in the following section.

Theoretical Results from Model Calculations

Ground-State Geometries. The intermolecular forces in pyridine clusters arise not only from dispersion forces. There are also electrostatic interactions, which are due to the molecular dipole and quadrupole moments. Different intermolecular orientations are possible, as shown in recent calculations on pyridine clusters (see Figure 4).[32] This implies that various isomers of variable-size clusters are considered in this work. This also explains the complicated X-ray structure and indicates the occurrence of several phases in the solid state, where all molecular 2-fold axes are nearly parallel to one basal plane of the orthorhombic lattice, corresponding to the space group $Pna2_1$.[36–38]

The most stable dimer structure is found according to ab initio calculation and previous work[32] to be an antiparallel displaced C_{2h} structure, where the nitrogen sites are on opposite sides, as shown in Figure 4b. This intermolecular configuration is reasonable to be the most stable dimer structure, considering the intermolecular dipole−dipole interaction. It can also be seen as a result of electrostatic interactions that the partially positively charged hydrogen sites of one ring lies on top of the partially negatively charged nitrogen site of the other ring. The intramolecular C−N distance is found to be 1.345 Å, the C−C distance

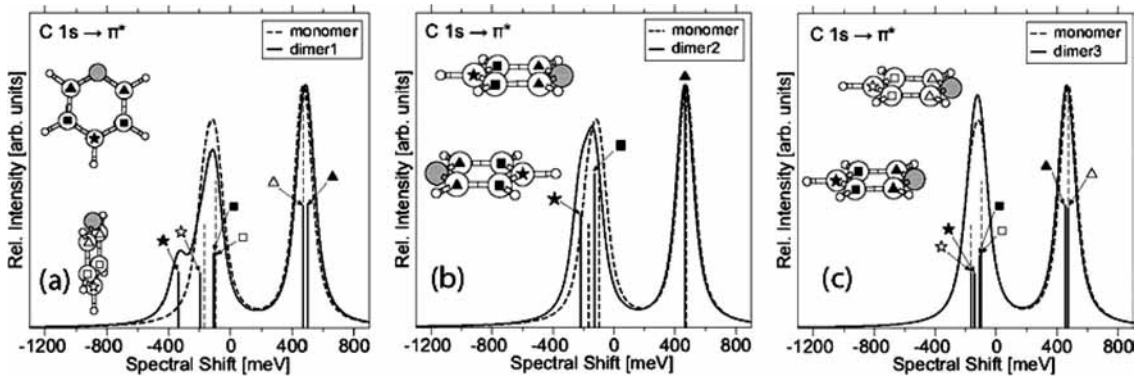

Figure 4. Simulated C 1s→π^* ($\upsilon = 0$) transition of molecular pyridine (dashed vertical lines and curves) and different isomers of the pyridine dimer (solid vertical lines and curves). The symbols indicate the different carbon sites and their excitation energies: (a) chain-like dimer isomer; (b) antiparallel displaced isomer; (c) parallel displaced isomer. The symbols mark equivalent sites. The data are plotted on an energy scale relative to molecular benzene.

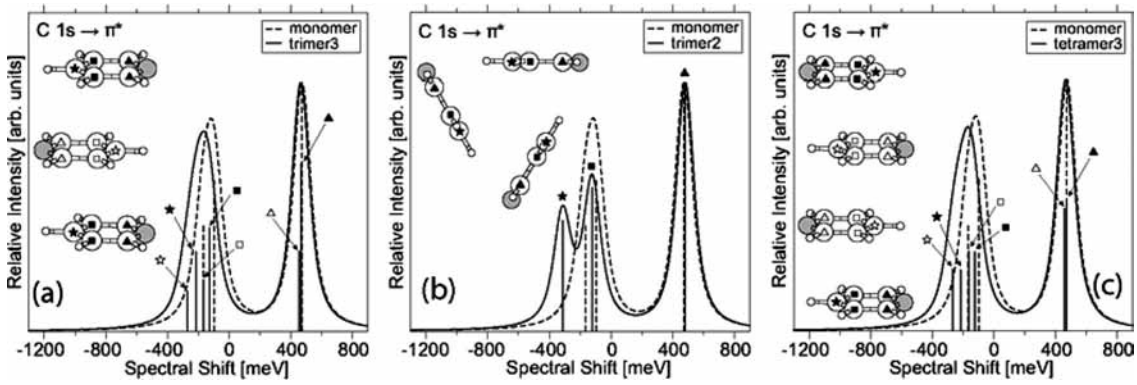

Figure 5. Simulated C 1s→π^* ($\upsilon = 0$) transition of molecular pyridine (dashed vertical lines and curves) and different isomers of the pyridine trimer and tetramer (solid vertical lines and curves). The symbols mark equivalent sites. The data are plotted on an energy scale relative to molecular benzene.

is 1.395 Å, and the C−H distance is 1.087 Å. The center-of-mass distance between both rings is 3.32 Å in the perpendicular direction and is displaced by 1.24 Å along the molecular planes, which is similar to previous results.[32] In addition, we have also considered chain-like structures. An energy minimum is found only for a dimer, where the intermolecular bonding occurs between a nitrogen atom of one ring and a hydrogen site of the other ring, as shown in Figure 4a. In this case, the N−H distance is 2.40 Å, and the center of mass distance between the two rings is 6.29 Å. Furthermore, we attempted to calculate a stable T-shaped isomer, but this is not possible. Instead, we find a π-stacking isomer, which is parallel displaced, where the centers of both rings are displaced relative to the other one, as shown in Figure 4c.

In the case of pyridine trimers, antiparallel displaced isomers are stable, similarly to ref 32 (cf. Figure 5a). When starting from the configuration of the cyclic benzene trimer, evidence for stable cyclic trimers is provided. The cyclic trimer with the N atoms pointing away from the other pyridine molecules is found to be more stable by 89 meV/molecule than the cyclic trimer with the N atoms pointing toward the center of another pyridine molecule. Thus, the latter isomer is not discussed any more. Finally, the trimer shown in Figure 5b is more stable by 28 meV/molecule than the antiparallel displaced trimer.

In the case of pyridine tetramers, the antiparallel displaced isomer is found to be the most stable one, as shown in Figure 5c. This sandwich-like structure is stable because of the intermolecular electrostatic interactions that are also observed for the dimers and trimers. Furthermore, the pyridine tetramer is optimized by starting from the crystallographic structure of pyridine in the (001) plane, where all dipoles are arranged in a nearly planar layer.[38] The resulting isomer is face-triangular tetramer, similar in structure to the benzene tetramer.[20] It is, however, less stable than the antiparallel displaced isomer shown in Figure 5c.

C 1s→π^* Regime. We have calculated the C 1s→π^* excitation energies as well as the C 1s ionization energies of pyridine and its cluster by using the different isomers discussed above. The molecular C 1s ionization energies are calculated to be 291.585, 290.652, and 291.191 eV for the carbon centers relative to the nitrogen site, labeled 2 (ortho), 3 (meta), and 4 (para), respectively. These values are similar to earlier theoretical work.[23] On the other hand, the C 1s→π^* excitation energy is calculated to be 286.722 eV (ortho), 286.152 eV (meta), and 286.082 eV (para) with oscillator strengths of 0.0195 (ortho), 0.00119 (meta), and 0.0168 (para), respectively. The present results indicate that transition energies are systematically somewhat higher than the experimental ones (cf. Figure 1). Each calculated excitation is broadened by a Voigt profile. This contains a Gaussian line width of 60 meV and a Lorentzian line width of 110 meV, which is mostly determined by the core hole lifetime. Note that this assumption is quite realistic, considering the instrumental resolution, as determined from additional calibration experiments, where 40 meV are derived for the C 1s regime and 60 meV for the N 1s regime. The Gaussian line width is essentially due to the bandwidth of the X-ray monochromator. Furthermore, the calculations do not take vibronic fine structure into account. As a result, the simulated line shapes correspond only to the C 1s→π^* ($\upsilon = 0$) transitions, which occur at the low-energy part of each experimental 1s→π^*

band. This is different from previous work, where the entire C 1s→π^* band was simulated by different fitting models.[23] Because there are only minor changes in spectral shape, we focus in this work on the C 1s→$\pi^*(\nu = 0)$ transition. The molecular spectra are used as reference values, where a relative energy scale is used in order to visualize the energy shifts between the neat molecule and clusters. In the C 1s regime, benzene is used as a reference value, whereas in the N 1s regime, molecular pyridine is used. Figure 4b shows the comparison between the most stable dimer and the molecule. The ortho-carbon sites, corresponding to the higher-energy feature, show a negligible redshift relative to the molecular excitation. In contrast, the para-carbon site, corresponding to the lowest-energy feature of this band, shows a redshift of 54 meV, and the meta-carbon sites contributes to a redshift of 28 meV. This result is already qualitatively in agreement with the experimental results shown in Figure 1. The distinct spectral shifts of the different carbon sites reflect the experimental results, where the strongest shift is due to the para-carbon center. This corresponds to the substantial redshift of the low-energy slope of the lower portion of the C 1s→π^* band, whereas the high-energy slope of this feature is only slightly redshifted. This can be rationalized by contributions from the meta-carbon sites. The high-energy portion of the band shows a smaller spectral shift, which can be explained by the ortho-carbon centers. It is clear that the experimental results cannot be fully explained by the most stable dimer isomer. Therefore, the spectral simulations of other isomers and larger clusters are considered, as well.

Figure 4a shows the calculated spectra of the C 1s→ π^* ($\nu = 0$) excitation of the chain-like dimer. This leads to nondegenerate transition energies for the different positions of the carbon sites (ortho, meta, and para), which is unlike the situation of the most stable isomer shown in Figure 4b. The C 1s excitation of the ortho-carbon sites yields a slight blueshift of the band. The meta-sites yield a slight redshift of the high-energy slope. Excitation of the para-carbon, which interacts with the nitrogen from the other molecule in the dimer, shows a substantial redshift (marked by ★ in Figure 4a). This would result in a distinct shoulder in the experimental spectra and indicate that this isomer is likely not present in the jet.

Figure 4c shows the calculated spectrum of the C 1s→π^* excitations in the parallel displaced pyridine dimer, which is the most unstable of the three isomers. The excitation at the ortho- and meta-sites are redshifted, whereas the excitation at the para-site is slightly blueshifted relative to the excitation in the molecule. This is unlike the experimental results, which also indicates that this isomer is likely not present in the jet. However, low mixing ratios of various isomers cannot be excluded to occur in the jet expansion.

The C 1s spectra of the trimer are simulated in the same way as the dimer. The results are shown in Figure 5a,b. The spectral simulation for the most stable antiparallel trimer is shown in Figure 5a. Similarly to the antiparallel dimer as shown in Figure 4b, all the transitions are redshifted relative to the excitations in the isolated molecule. The smallest redshift is observed for the ortho-carbon sites, which is in qualitative agreement with the experimental results. In contrast, the spectral redshift of the other carbon sites is considerably larger. Specifically, in the sandwiched middle pyridine, the para-carbon site shows a 105 meV redshift. This redshift is smaller (47 meV) for the meta-carbon sites. It is also evident from Figure 5a that the low-energy slope of the low-energy feature containing the C 1s→π^* (para, meta) transitions shows a larger redshift than the high-energy slope of this spectral feature. The shift of 105 meV for this para-site indicates that the magnitude of the redshift changes from surface to bulk, where the middle molecule resembles bulk sites. Its magnitude is indeed comparable to the experimental results shown in Figure 1. This shift is also larger than that for the dimer simulations (cf. Figure 4b) and indicates that larger clusters than dimers contribute to the experimental results. Figure 5b shows the spectral simulation of the C 1s→π^* transition of a symmetric cyclic trimer. A slight blueshift of the high-energy feature, corresponding to the ortho-carbon, is observed, which is similar to that of the chain-like dimer, as shown in Figure 4a. Most significant is the redshift of the para-sites. A shift of 148 meV is calculated for this site. This indicates that a split signal, or at least a significantly broadened spectral feature, should occur in the experimental results, if such trimers are present. However, the sum of all spectral features is not in agreement with the experimental findings. Therefore, the occurrence of significant mixing ratios of a cyclic trimer in the cluster jet is discounted.

Figure 5c shows the most stable tetramer along with a spectral simulation. Only one isomer is considered, because the above-discussed dimers and trimers indicate that only the most stable species yield agreement with the experimental findings shown in Figure 1. The results indicate that all transitions are redshifted relative to the neat molecule. Similarly to the trimer, one finds the smallest spectral shift for ortho-sites. In the sandwiched two pyridine molecules, the para-carbon sites show 100 meV redshift, which is smaller for the meta-carbon sites (52 meV). These values are nearly the same as those for the antiparallel trimer shown in Figure 5a, underlining the occurrence of these species in the jet. This indicates that the second-nearest neighbor pyridine is only contributing a little to the C 1s→π^* excitation of a target pyridine that is bound in clusters with an antiparallel stacked geometry.

N 1s→π^* Regime. The molecular N 1s→$\pi^*(b_1)$ ($\nu = 0$) transition is calculated to occur at 399.245 eV. This value is somewhat higher than the experimental value, which corresponds to the maximum of the Franck−Condon profile (see Figures 2 and 3 and refs 23 and 31). The calculated N 1s ionization energy is 404.396 eV, yielding a term value of the N 1s→$\pi^*(b_1)$ transition of 5.15 eV, which is somewhat lower than what was communicated in previous work.[31,39] The results clearly indicate that there is good agreement of the calculated N 1s ionization energy with the experimental value, which is known to be 404.9 eV.[40]

We focus here, as in the C 1s regime, on energy shifts in dimers and trimers relative to the molecular 1s→$\pi^*(\nu = 0)$ transition. No attempt is made to model the entire band profile. Each calculated transition is broadened by a Voigt profile, similar to the C 1s→$\pi^*(\nu = 0)$ transition discussed in the previous section. The Voigt profile consists of a Gaussian line width of 60 meV and a Lorentzian line width of 120 meV. This considers the bandwidth of the X-ray monochromator and the core hole lifetime. Note that the oscillator strengths of the 1s→π^* transitions does not change in clusters compared with the isolated molecule, which is similar to the C 1s regime.

Figure 6 shows the calculated spectrum of the N 1s→$\pi^*(\nu = 0)$ transition. Three isomers are considered, where the most stable one is the antiparallel displaced isomer shown in Figure 6b. Both nitrogen sites are equivalent. The calculated N 1s→$\pi^*(\nu = 0)$ transition is blueshifted by 44 meV relative to the isolated molecule. Figure 6a shows the calculated dimer spectrum of the N 1s→π^* transition in the chain-like structure. The transition is somewhat less blueshifted, where a value of 33 meV relative to the excitation in the isolated molecule is

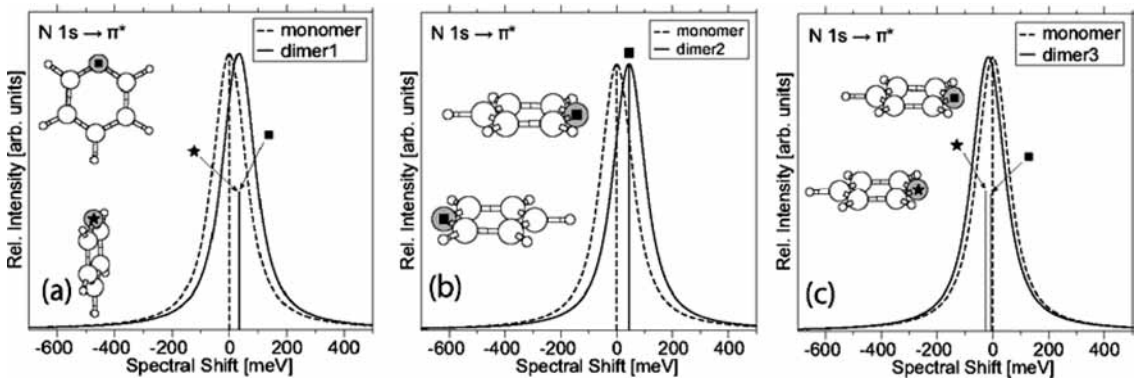

Figure 6. Simulated N 1s→π^* ($\upsilon = 0$) transition of molecular pyridine (dashed vertical lines and curves) and different isomers of the pyridine dimer (solid vertical lines and curves). The symbols mark equivalent sites. The data are plotted on an energy scale relative to molecular pyridine.

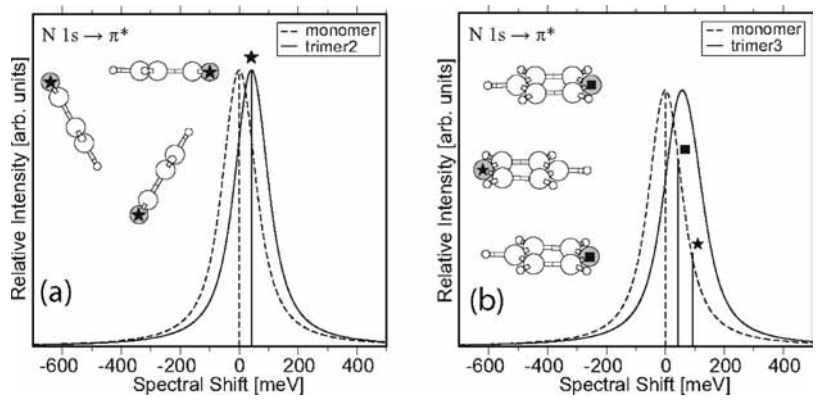

Figure 7. Simulated N 1s→π^* ($\upsilon = 0$) transition of molecular pyridine (dashed vertical lines and curves) and different isomers of the pyridine trimer (solid vertical lines and curves). The symbols mark equivalent sites. The data are plotted on a relative energy scale relative to molecular pyridine.

derived. Figure 6c shows the calculated spectrum of the N 1s→π^* excitation in the parallel displaced dimer, which consists of two inequivalent nitrogen sites. Spectral broadening yields an averaged value of the spectral shift of the N 1s→π^* ($\upsilon = 0$) transition, which is redshifted by 15 meV relative to the molecular transition.

Considering the experimental results shown in Figures 2 and 3 yields the following situation. The experimental blueshift only resembles the results on the antiparallel dimer and chain-like isomer. The calculated blueshift is in all the dimer cases that are considered here smaller than that in the experimental results. This is similar to the C 1s regime and indicates that larger clusters contribute to the experimental spectral shifts.

Clusters larger than the dimer are also modeled in the N 1s regime. Figure 7 shows typical examples of spectral simulations on the N 1s→π^* ($\upsilon = 0$) transition in the cyclic (Figure 7a) and the antiparallel trimer (Figure 7b). Both isomers yield spectral blueshifts but of different magnitude. Figure 7a shows that there is a 42 meV blueshift relative to the molecule. This is still smaller than in the antiparallel trimer. The sandwiched middle pyridine molecule yields a 91 meV blueshift. In contrast, the outer pyridine molecules show the same blueshift of 44 meV as the antiparallel dimer. Comparing these calculated values to the experimental results indicates that the antiparallel isomers are dominant. Furthermore, the magnitude in experimental blueshifts of 85 ± 15 meV (see Figure 2) and 95 ± 15 meV (see Figure 3) indicates that there is a small size-dependent spectral shift in the N 1s regime. This is explained by the size-dependent ratio of molecules that are bound on the surface and in the bulk of clusters. Additional calculations have been performed on the N 1s→π^* transition of the most stable tetramer (simulations not shown, where the assumed structure corresponds to Figure 5c). The antiparallel displaced isomer reveals two distinctly blueshifted features, where the interior, sandwiched pyridine molecules contribute to a blueshift of 92 meV, and there is a 50 meV blueshift for the outer molecules. The broadened band reveals a calculated overall blueshift of 72 meV, which is slightly smaller than the experimentally determined value. This result indicates that there are only minor changes in spectral shift upon cluster growth, if such stable, sandwich-like structures dominate in the regime of microclusters. Note that other cyclic isomers of the tetramer have been modeled, as well. These are also found to correspond to local minima, but they are less stable than the isomer shown in Figure 5c. However, they contribute only to smaller blueshifts to the N 1s→π^* transition (<50 meV) so that their contribution to the experimental results appears to be less important. Finally, we conclude that the inner molecules, corresponding to bulk sites in antiparallel stacked structures, give rise to the largest spectral shift, similarly to the results on C 1s excited pyridine clusters. This view is also consistent with additional calculations of the N 1s excited pyridine trimer and tetramer, where also different isomers are considered. Similarly to the C 1s edge, these support the assignments given above; therefore, these results are not discussed in greater detail.

Origin of the Spectral Shifts. Spectral shifts of core-to-valence transitions occurring in free clusters have been identified before.[16–20] In the pre-edge regime, only redshifts have been observed to date, which is unlike Rydgberg/exciton transitions.[12–15] A redshift corresponds to a stabilization of the transition in

TABLE 1: Calculated 1s→π* Excitation Energy *E* (in eV) and Energy Shift Δ*E* (in meV) in Antiparallel Stacked Pyridine Dimer and Trimer (Center Molecule)[a]

		dimer (Δ*E* [meV])			trimer (Δ*E*) [meV]
	molecule *E* [eV]	point charge	frozen	Hartree−Fock	Hartree−Fock
N	399.245	+47	+41	+44	+91
C(ortho)	286.722	−30	−45	−54	−105
C(meta)	286.152	−0	−2	−5	−13
C(para)	286.082	−10	−25	−28	−47

[a] Δ*E* (point charge) is evaluated by using point charges for neighboring pyridine(s), and Δ*E* (frozen) is evaluated by freezing the wavefunctions of the isolated systems.

clusters compared to the isolated molecule. Such stabilization has been rationalized by previous ab inito calculations as well as complimentary work by using the quasi-atomic approach.[16–19] The latter one indicates that the stabilization is due to dynamic processes that have been associated with dynamic core-hole localization.[16,17] Moreover, in the case of shape resonance, changes in single-hole ionization cross section have been discussed.[18] These affect size-dependently a double barrier surroundings in a cluster in cage-like molecules, such as SF_6, and contribute to small spectral shifts. The spectral changes in the C 1s regime are in full accordance with previous work on C 1s excited benzene clusters,[20] where site-dependent spectral shifts have been identified via ab inito calculations. These contribute to the overall spectral shifts that are observed in the experiments. Stabilization is evidently related to the number of neighboring sites, which are linked to the absorbing atom via intermolecular interactions.

The present work, however, clearly shows that destabilization processes can also be observed in near-edge spectra. First experimental evidence comes from N 1s→π* excited pyridine clusters. This observation contrasts sharply with the case of the C 1s→π* excitation. There are several types of intermolecular interactions. These include electrostatic (Coulomb), exchange, charge transfer (delocalization), and dispersion (van der Waals) interactions. In general, we have to discuss a spectral shift Δ*E* in terms of an energy difference between the ground state and core-excited state. Both states are neutral, and the π* orbital is not at all diffusing over to the neighboring molecules. This is due to the present model, where we have neglected dispersion interactions in the present calculations. Interestingly, we have derived semiquantitatively reasonable energy shifts in clusters, which compare well with the experimental results. Thus, we need to discuss the other mentioned sources of intermolecular interactions in greater detail in order to assign the dominant contribution to the spectral shifts. The transition energies, evaluated by freezing noninteracting wave functions, can be compared with those evaluated by relaxing them, which correspond to Hartree−Fock ones. However, even the former ones should be evaluated by orthogonalizing the wave functions with each other to satisfy the Pauli exclusion principle, which involves exchange interactions in addition to electrostatic interactions. Table 1 compares the energy shifts for the antiparallel stacked dimer and trimer, where only the central molecule is considered in the trimer. The shifts for the frozen and relaxed wave functions are almost the same in the dimer, indicating that the electrostatic interactions without changes in the wave functions are essential. This implies that the overlap and exchange interactions between the ground and core-to-valence excited molecules should be small.

In addition, electrostatic interactions are also evaluated in another way, as shown in Table 1. One can use point charges for neighboring molecules, so that reasonable energy shifts are derived. This implies that the wave functions have no overlap. In the present work, the one-electron electrostatic potential of the ground state of a pyridine molecule is fitted by putting a point charge on each atom. As shown in Table 1, the point-charge approximation using the atomic charges derived from the electron density of the neighboring molecule is not complete but is qualitatively reasonable to simulate site-dependent spectral shifts, where large or small values as well as redshifts or blueshifts are reasonably derived. The present results highlight the fact that the energy shift in the core→π* excitation is mainly due to electrostatic interactions in the case of the polar pyridine molecule.

Conclusions

Experiments on core-excited pyridine clusters show that there is first evidence for site- and element-selective stabilization and destabilization in free variable-size clusters. This is evidenced by 1s→π* transitions. The C 1s excited clusters give evidence for a stabilization shift (spectral redshift), which is dependent on the geometrical site. Therefore, distinct spectral shifts are observed for ortho-, meta-, and para-carbon sites. In contrast, the N 1s excitation shows a considerable destabilization (spectral blueshift) of the N 1s→π* transition in clusters relative to the isolated molecule. Ab initio calculations are applied in order to rationalize these experimental results. Geometry optimizations indicate that the ground state of pyridine dimers, trimers, and tetramers are electrostatically stabilized with the molecular dipole antiparallel to each other. Spectral simulations of the 1s→π* transitions indicate that only the most stable isomers with antiparallel stacked geometries give the best agreement with the experimental results of site- and size-dependent spectral redshifts and blueshifts. This means that the antiparallel isomers are preferably present in the present experimental conditions. The site-dependent blueshifts and redshifts in core-to-π* excitations of antiparallel isomers are revealed to be results of electrostatic intermolecular interactions between the polar pyridine molecule.

Acknowledgment. Financial support by the Deutsche Forschungsgemeinsachaft (RU 420/8-1) and the Fonds der Chemischen Industrie is gratefully acknowledged.

References and Notes

(1) Lee, E. C.; Kim, D.; Jurečka, P.; Tarakeshwar, P.; Hobza, P.; Kim, K. S. *J. Phys. Chem. A* **2007**, *111*, 3446.
(2) Brutschy, B. *Chem. Rev.* **2000**, *100*, 3891.
(3) Burley, S. K.; Petsko, G. A. *Science* **1985**, *229*, 23.
(4) Hoeben, F. J. M.; Jonkheijm, P.; Meijer, E. W.; Schenning, A. P. H. J. *Chem. Rev.* **2005**, *105*, 1491.
(5) Fenniri, H.; Deng, B.-L.; Ribbe, A. E.; Hallenga, K.; Jacob, J.; Thiyagarajan, P. *Proc. Nat. Acad. Sci. U.S.A.* **2002**, *99*, 6487.
(6) (a) Rühl, E.; Bisling, P. G. F.; Brutschy, B.; Baumgärtel, H. *Chem. Phys. Lett.* **1986**, *126*, 232. (b) Brutschy, B.; Bisling, P.; Rühl, E.; Baumgärtel, H. *Z. Physik D* **1987**, *5*, 217.
(7) Bouvier, B.; Millié, P.; Mons, M. *J. Phys. Chem. A* **2004**, *108*, 4254.
(8) Han, S. Y.; Song, J. K.; Kim, J. H.; Oh, H. B.; Kim, S. K. *J. Chem. Phys.* **1999**, *111*, 4041.
(9) Card, D. A.; Wisniewski, E. S.; Folmer, D. E.; Castleman, A. W., Jr *J. Chem. Phys.* **2002**, *116*, 3554.
(10) Le Barbu, K.; Schiedt, J.; Weinkauf, R.; Schlag, E. W.; Nilles, J. M.; Xu, S.-J.; Thomas, O. C.; Bowen, K. H. *J. Chem. Phys.* **2002**, *116*, 9663.
(11) Rühl, E. *Int. J. Mass Spectrom. Ion Proc.* **2003**, *229*, 117.
(12) (a) Rühl, E.; Heinzel, C.; Hitchcock, A. P.; Baumgärtel, H. *J. Chem. Phys.* **1993**, *98*, 2653. (b) Pavlychev, A. A.; Semenova, E. V.; Hitchcock, A. P.; Rühl, E. *Physica B* **1995**, *208−209*, 187.
(13) Björneholm, O.; Federmann, F.; Fössing, F.; Möller, T. *Phys. Rev. Lett.* **1995**, *74*, 3017.

(14) Knop, A.; Wassermann, B.; Rühl, E. *Phys. Rev. Lett.* **1998**, *80*, 2302.
(15) Flesch, R.; Kosugi, N.; Bradeanu, I. L.; Neville, J. J.; Rühl, E. *J. Chem. Phys.* **2004**, *121*, 8343.
(16) Flesch, R.; Pavlychev, A. A.; Neville, J. J.; Blumberg, J.; Kuhlmann, M.; Tappe, W.; Senf, F.; Schwarzkopf, O.; Hitchcock, A. P.; Rühl, E. *Phys. Rev. Lett.* **2001**, *86*, 3767.
(17) Pavlychev, A. A.; Flesch, F.; Rühl, E. *Phys. Rev. A* **2004**, *70*, 015201.
(18) Pavlychev, A. A.; Brykalova, X. O.; Flesch, R.; Rühl, E. *Phys. Chem. Chem. Phys.* **2006**, *8*, 1914.
(19) (a) Pavlychev, A. A.; Rühl, E. *J. Electron Spectrosc. Relat. Phenom.* **2000**, *106*, 207. (b) Pavlychev, A. A.; Rühl, E. *J. Electron Spectrosc. Relat. Phenom.* **2000**, *107*, 203.
(20) Bradeanu, I. L.; Flesch, R.; Kosugi, N.; Pavlychev, A. A.; Rühl, E. *Phys. Chem. Chem. Phys.* **2006**, *8*, 1906.
(21) Menzel, D.; Rocker, G.; Steinrück, H.-P.; Coulman, D.; Heimann, P. A.; Huber, W.; Zebisch, P.; Lloyd, D. R. *J. Chem. Phys.* **1992**, *96*, 1724.
(22) Rühl, E.; Schmale, C.; Jochims, H. W.; Biller, E.; Simon, M.; Baumgärtel, H. *J. Chem. Phys.* **1991**, *95*, 6544.
(23) Kolczewski, C.; Püttner, R.; Plashkevych, O.; Ågren, H.; Staemmler, V.; Martins, M.; Snell, G.; Schlachter, A. S.; Sant'Anna, M.; Kaindl, G.; Pettersson, L. G. M. *J. Chem. Phys.* **2001**, *115*, 6426.
(24) Smalley, R. E.; Wharton, L.; Levy, D. H. *Acc. Chem. Res.* **1977**, *10*, 139.
(25) Frisch, M. J.; Trucks, G. W.; Schlegel, H. B.; Scuseria, G. E.; Robb, M. A.; Cheeseman, J. R.; Montgomery, J. A., Jr.; Vreven, T.; Kudin, K. N.; Burant, J. C.; Millam, J. M.; Iyengar, S. S.; Tomasi, J.; Barone, V.; Mennucci, B.; Cossi, M.; Scalmani, G.; Rega, N.; Petersson, G. A.; Nakatsuji, H.; Hada, M.; Ehara, M.; Toyota, K.; Fukuda, R.; Hasegawa, J.; Ishida, M.; Nakajima, T.; Honda, Y.; Kitao, O.; Nakai, H.; Klene, M.; Li, X.; Knox, J. E.; Hratchian, H. P.; Cross, J. B.; Bakken, V.; Adamo, C.; Jaramillo, J.; Gomperts, R.; Stratmann, R. E.; Yazyev, O.; Austin, A. J.; Cammi, R.; Pomelli, C.; Ochterski, J. W.; Ayala, P. Y.; Morokuma, K.; Voth, G. A.; Salvador, P.; Dannenberg, J. J.; Zakrzewski, V. G.; Dapprich, S.; Daniels, A. D.; Strain, M. C.; Farkas, O.; Malick, D. K.; Rabuck, A. D.; Raghavachari, K.; Foresman, J. B.; Ortiz, J. V.; Cui, Q.; Baboul, A. G.; Clifford, S.; Cioslowski, J.; Stefanov, B. B.; Liu, G.; Liashenko, A.; Piskorz, P.; Komaromi, I.; Martin, R. L.; Fox, D. J.; Keith, T.; Al-Laham, M. A.; Peng, C. Y.; Nanayakkara, A.; Challacombe, M.; Gill, P. M. W.; Johnson, B.; Chen, W.; Wong, M. W.; Gonzalez, C.; Pople, J. A. *Gaussian 03*, revision C.02; Gaussian, Inc.: Wallingford, CT, 2004.
(26) Kosugi, N.; Kuroda, H. *Chem. Phys. Lett.* **1980**, *74*, 490.
(27) Kosugi, N.; Kuroda, H. *Chem. Phys. Lett.* **1983**, *94*, 377.
(28) Kosugi, N. *Theor. Chim. Acta* **1987**, *72*, 149.
(29) Huzinaga, S.; Andzelm, J.; Klobukowski, M.; Radzio-Andzelm, E.; Sakai, Y.; Tatewaki, H. *Gaussian Basis Sets for Molecular Calculations*; Elsevier: Amsterdam, 1984.
(30) Schmid, R. P.; Jäckel, J.-G.; Jones, H.; Taubmann, G.; Takeo, H. *Int. J. Mass Spectrom.* **1998**, *177*, 197.
(31) Hannay, C.; Duflot, D.; Flament, J.-P.; Hubin-Franskin, M.-J. *J. Chem. Phys.* **1999**, *110*, 5600.
(32) Piacenza, M.; Grimme, S. *ChemPhysChem* **2005**, *6*, 1554.
(33) Hagena, O. F.; Obert, W. *J. Chem. Phys.* **1972**, *56*, 1793.
(34) Rühl, E.; Brutschy, B.; Baumgärtel, H. *Chem. Phys. Lett.* **1989**, *157*, 379.
(35) Gotts, N. G.; Lethbridge, P. G.; Stace, A. J. *J. Chem. Phys.* **1992**, *96*, 408.
(36) Biswas, S. G. *Indian J. Phys.* **1958**, *32*, 13.
(37) Castellucci, E.; Sbrana, G.; Verderame, F. D. *J. Chem. Phys.* **1969**, *51*, 3762.
(38) Mootz, D.; Wussow, H.-G. *J. Chem. Phys.* **1981**, *75*, 1517.
(39) Horsley, J. A.; Stöhr, J.; Hitchcock, A. P.; Newbury, D. C.; Johnson, A. L.; Sette, F. *J. Chem. Phys.* **1985**, *83*, 6099.
(40) Bakke, A. A.; Chen, H. W.; Jolly, W. L. *J. Electron Spectrosc. Relat. Phenom.* **1980**, *20*, 333.

JP802068H